Manipulating the Optical Properties of Carbon Dots by Fine-Tuning their Structural Features

Manipulating the optical properties of carbon dots via fine tuning their structural features

Hui Luo,[a, j] Nikolaos Papaioannou,[b, c] Enrico Salvadori,[d, e] Maxie Roessler,[e] Liviu Tanase,[f] Jingyu Feng,[a, j] Yiwei Sun,[c] Yan Yang,[a] Mohsen Danaie,[g] Ana Sobrido,[a, b] Andrei Sapelkin,[b, c] James Durrant,[h] Stoichko D. Dimitrov[i]* and Maria-Magdalena Titirici[a, b, j]*

The term "carbon dots" represents an "umbrella term" as there are many classes of materials included. We show how by fine tuning the structural features of hydrothermally synthesized carbon dots using simple reduction/oxidation reactions we can drastically affect their excited state properties. Increasing the surface C=O groups leads to a higher photoluminescence quantum yield, while a higher density of graphene-like domains results in an order of magnitude weaker photoluminescence. Structural and spectroscopic studies including femtosecond transient absorption and time-correlated single photon counting experiments were employed to elucidate the excited state dynamics of the carbon dots. We have found that the photoluminescence originates from the direct excitation of localized fluorophores involving C=O functional groups, which act as individual emissive centers, while the excitation at the graphene-like structural features leads to ultrafast phonon-assisted relaxation to the ground state largely quenching the photoluminescence quantum yields. This comprehensive investigation sheds light on how understanding the excited state relaxation processes in different carbon dots structures is crucial for tuning the optical properties for any potential commercial applications.

Introduction

Carbon dots (CDs) is the generic name for a class of low-cost carbon nanomaterials, firstly reported in 2004,[1] possessing photoluminescent (PL) properties with an average particle size below 10 nm.[2] This category of carbonaceous materials are attractive for many applications ranging from bio-imaging to sensors, optoelectronics and more[3–6] due to their facile and inexpensive synthesis, low toxicity,[6] high (aqueous) solubility, optoelectronic properties, facile modification and stability against photo-bleaching.[7] Current synthetic approaches to produce CDs include top-down and bottom-up methods, which usually give aggregated graphene-like layers of various size and a large structural diversity including sp^2 / sp^3 carbon networks and oxygen rich functional groups at different ratios. As a result, the photoluminescence properties of CDs widely vary in quantum yields, from < 1 % to 95 % depending upon synthesis. Light excitation wavelength dependent and independent emission have been reported over the last decade.[8–11] Experimental and theoretical studies of CDs have revealed that photoluminescence originates predominantly from π-π* transitions involving hybridized orbitals from the sp^2 carbon core (amorphous and nanocrystalline) and functional C=O and COOH and C-O-C groups.[12,13] Radiative n-π* transitions involving carbon-oxygen surface groups are also thought to contribute to emission and can explain the observed solvent polarity and surface functionalization effects on light absorption and emission.[14,15] In addition, quantum confinement,[16] carbon cluster agglomeration and the formation of supramolecular aggregates[17] have also been reported demonstrating the great complexity of their optical absorption and emission properties and the need for fundamental studies to unlock their potential for semiconductor-like and biological applications.[18]

[a] School of Engineering and Materials Science, Queen Mary University of London, Mile End Road, E1 4NS, London, UK
[b] Materials Research Institute, Queen Mary University of London, Mile End Road, E1 4NS, London, UK
[c] School of Physics and Astronomy, Queen Mary University of London, Queen Mary University of London, Mile End Road, E1 4NS, London, UK
[d] Department of Chemistry and NIS Centre, University of Turin, Via Giuria 7, Turin 10125, Italy
[e] School of Biological and Chemical Sciences, Queen Mary University of London, Mile End Road, E1 4NS, London, UK
[f] National Institute of Materials Physics, Atomistilor 405A, 077125, Magurele-Ilfov, Romania
[g] Diamond Light Source Ltd., electron Physical Science Imaging Centre, Harwell Science and Innovation Campus, OX11 0DE, Didcot, UK
[h] Department of Chemistry and Centre for Plastic Electronics, Imperial College London, SW7 2AZ, London, UK
[i] SPECIFIC IKC, College of Engineering, Swansea University SA2 7AX, Swansea, UK
[j] Department of Chemical Engineering, Imperial College London, South Kinsington Campus, SE7 2AZ, London, UK
Corresponding authors e-mail: stoichko.dimitrov@swansea.ac.uk; m.titirici@imperial.ac.uk
Electronic Supplementary Information (ESI) available: [Experimental Procedures and Characterization Data & Supporting Figures]. See DOI: 10.1039/x0xx00000x

In this work, we focused on a specific member of the CDs family, namely CDs prepared via Hydrothermal Carbonization (HTC) of carbohydrates.[19] In HTC, carbohydrates are converted into micrometre-sized carbonaceous spheres via a process involving 5-hydroxymethylfurfural (5-HMF) formation, its "polymerization" via a nucleation-growth process and intermolecular dehydration. Simultaneously to the formation of the micrometre sized-sphere sediments in the aqueous phase, there is also a formation of CDs with a diameter of a few nanometres which have been shown to have crystalline domains despite the low carbonization temperatures. By treating these CDs isolated from the aqueous phase of the HTC process with oxidization and reduction agents, we induced changes in the crystalline structure and functional groups, which changed their optoelectronic properties. These steps were deliberately designed to create more graphene-like CDs with a lower density of oxygen functional groups in the reduced samples (r-CDs) and highly amorphous CDs with a higher density of oxygen motifs in the oxidized samples (o-CDs). The structures of the CDs were analysed using several structural techniques including HR-TEM, EPR, XPS, Raman, ^{13}C-NMR and FTIR which allowed us to build a detailed picture of the structure and chemistry of the CDs. Then, the photoluminescence properties of the CDs were studied and it was found that they vary significantly between samples, with o-CDs showing enhanced PL while r-CDs showing much weaker PL. These differences were analysed using femtosecond transient absorption (TA) spectroscopy and time-correlated single photon counting

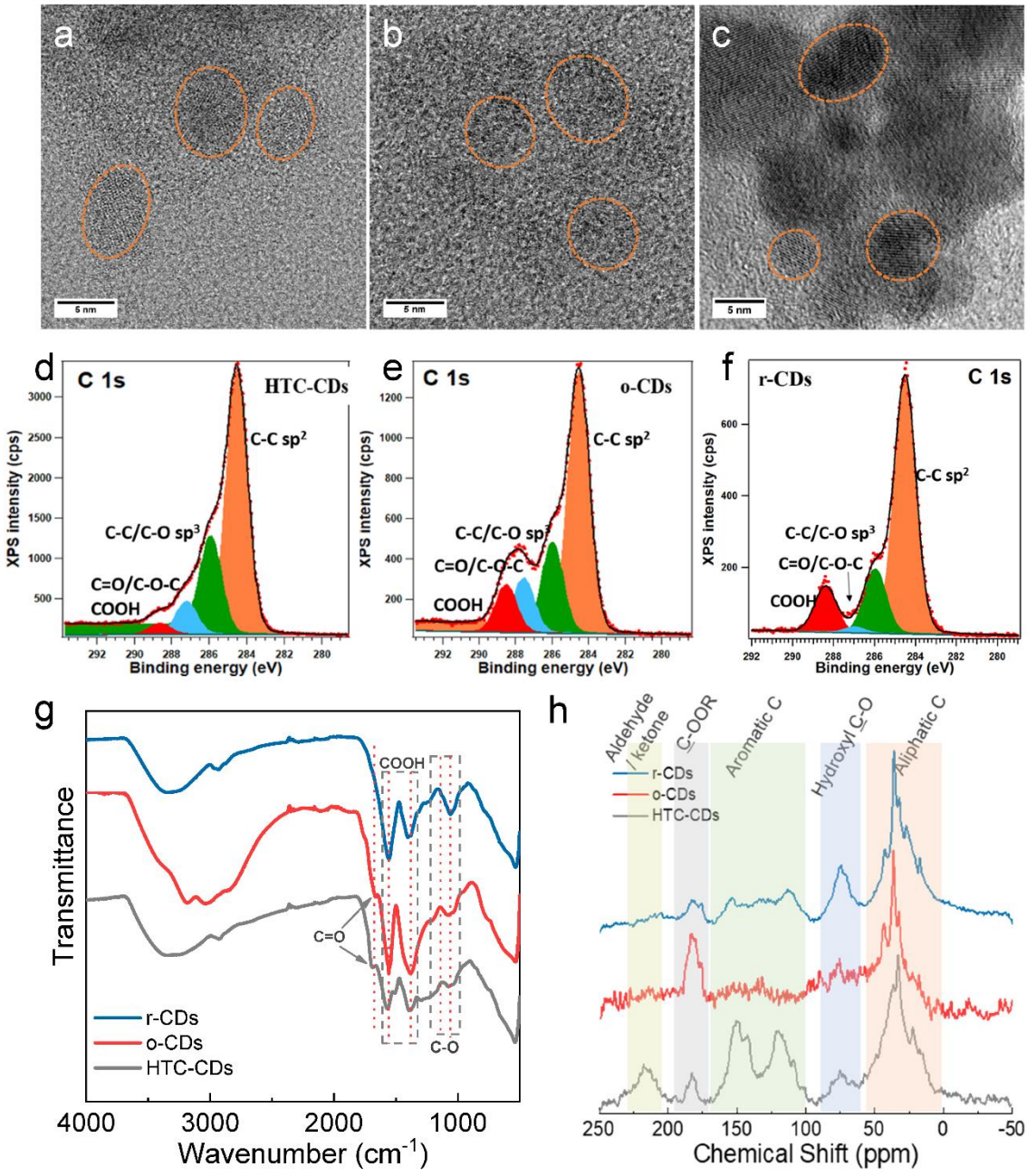

Figure 1 HR-STEM bright field images taken at 80 kV and C1s XPS spectra of (a, d) HTC-CDs, (b, e) o-CDs and (c,f) r-CDs; (g) corresponding FTIR spectra; (h) Solid state CP-MAS ^{13}C NMR spectra acquired at 12 kHz, pulse duration = 4.0 µs; recycle delay = 5s.

(TCSPC) which identified that the time scale of non-radiative excited state relaxation causing to PL quenching is picoseconds and that this quenching is mostly determined by the proportion of C=O versus C=C carbon in the dots.

Results and discussion

CDs were prepared via hydrothermal carbonization (HTC) of glucose,[20] by treating a 4% w/v aqueous glucose solution at 200 °C for 12 hours, followed by centrifugation and filtration to isolate the CDs from the larger carbon microspheres which simultaneously form during this process as explained above. The as-prepared CDs, named HTC-CDs here, appear as a yellow aqueous suspension that shows visible blue emission (around 450 nm) when illuminated by UV light. The HTC-CDs were then treated with oxidation (H_2O_2 / NH_4OH) and reduction ($NaBH_4$) agents for structural and optical properties studies, and the products are denoted as o-CDs and r-CDs, respectively. The o-CDs appear as a light-yellow solution while r-CDs show brown colour with the same concentration, both of which emit blue-green light upon UV excitation. The details regarding the preparation methods can be found in the experimental section.

Morphological characterization (**Figure 1a, b, c**) by high-resolution scanning transmission electron microscopy (HR-STEM) indicates that the as prepared HTC-CDs are about 5 nm in size and contain small lattice fragments embedded in an amorphous carbon matrix (**Figure S1**). Although the o-CDs and r-CDs have similar particle sizes, differences in the structure can be observed with o-CDs exhibiting more amorphous features and a higher degree of disorder, while the r-CDs show more graphitic features, with lattice fringes spaced by 0.24-0.29 nm which corresponds to the (001) crystal plane of graphite.[3]

Despite the morphological differences observed in HR-STEM, the Raman Spectra of HTC-CDs and r-CDs (acquired using 488 nm laser, **Figure S2**) display similar characteristics including a graphitic G band originating from the stretching of sp^2 carbon atoms and a weaker D band indicative of structural distortion of the graphitic sp^2 carbon layers with defects like sp^3 coordination or small dot size difference. Minor narrowing of the G band is noted from spectral fitting with a combination of Breit-Wigner-Fano (BWF) + Lorentzain line pair (**Table S1**),[21] indicating increased uniformity of the sp^2 graphitic carbon in the sample of r-CDs.

Table 1 Chemical composition in r-CDs, o-CDs and HTC-CDs extracted from the XPS data in **Figure 1**.

Sample	C-C sp^2	C-C/C-O sp^3	C=O	COOH
HTC-CDs	66%	23%	8%	3%
o-CDs	57%	20%	12%	11%
r-CDs	69%	17%	2%	12%

The XPS spectra of the CDs are presented in **Figure 1d, e, f** and their estimated bond compositions presented in **Table 1**. The XPS results identify that r-CDs have the highest percentage of sp^2 carbon among the three samples, which is in good agreement with our TEM and Raman analysis already suggesting a more graphitic core structure of the r-CDs than the other two CD types. HTC-CDs have slightly lower ratio of sp^2 carbon than r-CDs whilst o-CDs show only 57% of sp^2 carbon. Compared to o-CDs, the carbonyl groups in r-CDs are almost completely removed and instead COOH groups appear in the XPS spectra. In o-CDs we see the increase of both C=O and COOH groups, where the latter has a similar amount in o-CDs and r-CDs despite of the oxidation/reduction treatments. Detailed O1s spectra can be found in **Figure S3**.

Structural evidence can also be found from infrared (IR) spectroscopy, **Figure 1g**, where two major peaks for the

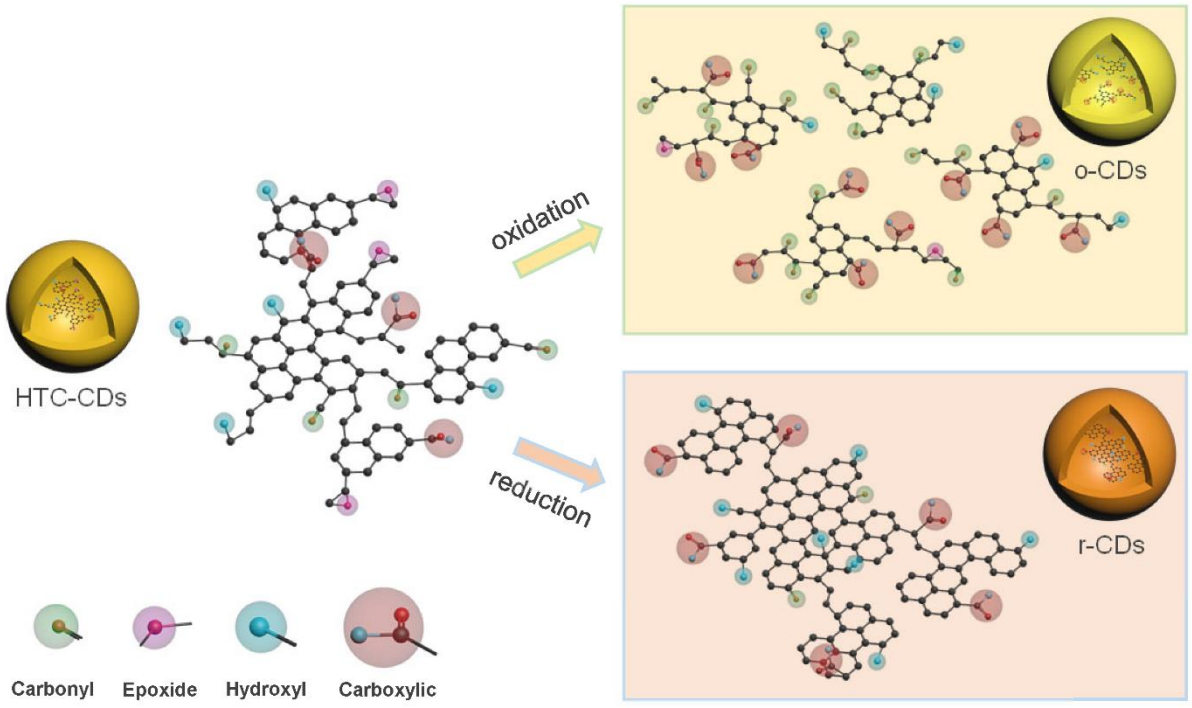

Scheme 1 Schematic diagram describing the structure evolution of carbon dots.

symmetric and antisymmetric stretches at 1569 cm^{-1} and 1376 cm^{-1} are assigned to COOH surface functionality.[22] Sub-peaks beside the two COOH peaks in HTC-CDs indicate there are other chemical bonds, but have been removed by the post-treatments. Two additional shoulder peaks at 1700 cm^{-1} are present in HTC-CDs and o-CDs and correspond to C=O stretches, which do not exist in r-CDs, matching the XPS results.

Solid state ^{13}C NMR analysis of CDs confirms the structural differences among different carbon dots, as shown in Figure 1h. Compared to the ^{13}C spectra of HTC-CDs, o-CDs show clear peaks at 0-70 ppm, indicating that the aliphatic carbon has remained after the oxidation process, while no obvious signal between 100-150 ppm showing that the aromatic rings have mostly disappeared. The ^{13}C NMR of o-CDs also shows relatively high proportion of R-COOR signal corresponding to a larger ratio of carboxyl groups in these dots. In comparison, the ^{13}C-NMR of r-CDs shows clear signatures of aromatic carbon, no signal from carbonyl groups and a clear signal from hydroxyl groups owing to the $NaBH_4$ reduction of C=O to C-OH, in excellent agreement with our XPS and FTIR analyses.

The differences in the structure and functionalities between the samples confirm that chemical oxidation and reduction tune the structure of hydrothermal CDs. Based upon our structural analysis, we can draw a representative scheme of the HTC-CDs, r-CDs and o-CDs, shown in **Scheme 1**. Upon the oxidation of HTC-CDs, a significant amount of oxygen is introduced into the dots, which leads to an increased concentration of C=O groups and decreased free radicals in the o-CDs. Upon reduction of HTC-CDs, the density of sp^2 graphitic carbon is increased creating r-CDs with a more extensive conjugated carbon network[23] and an order of magnitude smaller density of C=O. Furthermore, the removal of oxygen leaves more free radicals in r-CDs than in o-CDs. The HTC-CDs show "an in between" scenario where they have a moderate C/O ratio and C=O content.

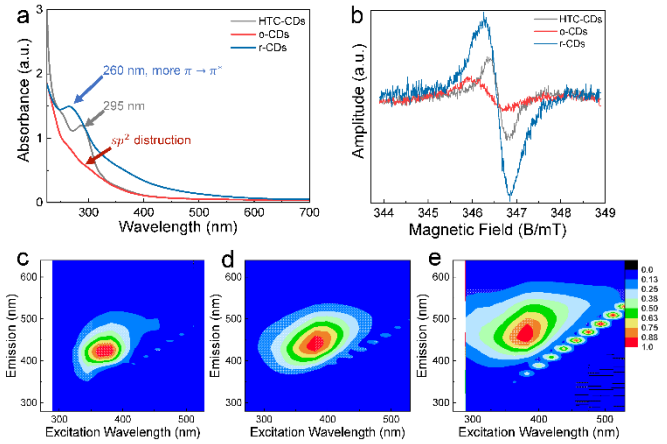

Figure 2 (a) UV-Vis absorbance of aqueous solutions of CDs (concentration: 0.1 mg/mL) and (b) EPR signal comparison of CD powders measured at room temperature; Photoluminescence maps of (b) HTC-CDs; (c) o-CDs; (d) r-CDs.

Figure 2a presents the UV-Vis absorbance spectra of HTC-CDs, r-CDs, and o-CDs dispersed in water with a concentration of 1 mg/ml. Each sample has a spectrum with a strong absorption towards the UV which tails off in the visible range.[24–26] The spectra show discernible differences between the samples signifying the impact of chemical reduction and oxidation on the optical properties of CDs. Comparing HTC-CDs to o-CDs, we observe that HTC-CDs display a clear peak at 295 nm (λ_{abs}) normally attributed to π-π* transitions within the sp^2 carbon core,[27] while for o-CDs this peak disappears and absorbance intensity monotonously decreases in the visible spectral region. This absorbance change in o-CDs is caused by the partial destruction of the sp^2 hybridization network upon oxidation, which decreases the probability for $\pi \rightarrow \pi^*$transitions, analogy to wide energy gap systems.[12,28] Compared to HTC-CDs, r-CDs have a well-defined absorption peak with a maximum at ~ 260 nm and much stronger visible absorption up to 650 nm which resembles much more closely the absorption of graphene and graphene oxide with narrower energy gaps and indicates a significant contribution from graphitic domains.[29–32] The energy gap changes based on sizes of sp^2 domains can be found in previous experimental and theoretical studies.[13,17,33]

Steady-state photoluminescence measurements as a function of excitation wavelength were carried out with all samples. The CDs exhibit excitation-dependent emission spectrum typical for CDs and which peaks in intensity at ~ 370 nm excitation (**Figure S6**).[14,34–37] Therefore, PL quantum yields (Φ) were recorded with a 370 nm excitation against a reference quinine sulphate solution.[38] The results show significant differences between each sample which are as follows: 1.82% for o-CD, 1.28% for HTC-CDs and 0.18% for r-CDs. This trend in Φ is another indicator of the strong impact of chemical treatment on the optical properties of HTC-CDs. Reduction with $NaBH_4$ leads to a significant drop in Φ likely caused by the increased graphitic character of r-CDs. Oxidation with H_2O_2 / NH_4OH leads to an increase in Φ coinciding with the reduction in the amount of graphitic carbon and the increase of C=O and COOH groups in o-CDs.[39–41] Furthermore, a direct comparison between Φ and the dot's composition according to the XPS results in **Table 1** shows that there is a direct correlation between the relative percentage ratio of C=O groups and Φ, indicating that the emissive excited states in the CDs synthesized here include C=O rather than COOH functional groups.

Figure 2c, d, e present normalized 3D-PL plots of each of the samples studied. They reveal that despite their big difference in Φ, the CDs and specifically o-CDs and r-CDs have nearly identical spectral features with a central PL peak at ~ 460 nm originating from an excitation at ~ 370 nm. This indicates that the origin of emission is from very similar excited states with an absorbance at ~ 370 nm not well-resolved in the UV-Vis absorbance spectra of the CDs and indicating a low concentration of the emissive fluorophores or low absorption coefficients. The data show that the strongest absorption < 300 nm in all CDs does not populate excited states, contributing strongly to PL. This is frequently observed for a variety of CDs and is related to their graphitic character inducing non-radiative phonon-assisted relaxation processes rather than excited state relaxation to emissive states.[24,25] A very similar peak broadening is observed for r-CDs and o-CDs further indicating that the origin of PL is due to the same excited states comprising of a common structural motif which we already identified to consist of C=O groups. The density of these motifs is clearly much higher in o-CDs than in r-CDs identifying that chemical reduction is disadvantageous for the production of strongly emissive CDs, whilst oxidation is clearly advantageous as seen from **Figure 3f**.

Another likely contributor to the dramatic change of quantum yield (Φ) in o-CDs and r-CDs is the radicals, which serve as traps for non-radiative recombination.[42,43] Continuous-wave EPR was used to obtain an estimate of the relative radical concentrations (by comparing normalized peak intensities) as well as a first indication of their chemical environment (based on the characteristic g values); **Figure 2b** reports experimental evidence on the three different compounds. From the intensity of the EPR spectra, after normalizing for sample mass and number of scans, the relative concentrations

follow the order r-CDs > HTC-CDs >> o-CDs. On the other hand $g_{\text{o-CDs}} > g_{\text{HTC-CDs}} > g_{\text{r-CDs}} > g_e$ = 2.0023 which, under the reasonable assumption that all CDs harbour π-radicals, suggests that o-CDs radical are more substituted with oxygen-containing groups than r-CDs.[44] The ratio between Φ_o/Φ_r is similar as the intensity ratio of r-CDs vs o-CDs, which offers good indication of the effect of free radicals on the PL. Akin to the case of fluorescent silicon nanocrystals, free radicals can act as surface defects and have a negative effect on PL.[43] A deeper insight into the chemical structure of these radicals is provided by pulse EPR experiments that measure the hyperfine coupling between electron and nuclear spins. HYSCORE experiments show an extended conjugated network in r-CDs compared to HTC-CDs around the paramagnetic defects (**Figure S4 and S5**), in good accordance with bulk spectroscopies such as NMR and FTIR that inform on the average structure of CDs.

on the nanosecond time scale are not fully indicative of the whole emission dynamics of HTC-CDs.[42,46,47] Possible reasons for this behaviour include static quenching or faster picosecond non-radiative relaxation of the excited states.[42] The decays in **Figure S7** show that the PL on the hundreds of picosecond and nanosecond timescales is mostly wavelength independent, supporting the conclusion that PL originates from individual excited states (fluorophores) not interacting with each other *via* energy or charge transfer processes,[42] and that ultrafast sub-nanosecond non-radiative recombination or ground state complexes determine the dots PL properties including their Stokes shift.[12]

Femtosecond transient absorption (TA) spectroscopy was used to shed light on the excited state dynamics in the CDs on the sub-nanosecond timescale. The samples were studied using 360 nm 100 fs laser pulses and 430-700 nm broadband probe light. **Figure 3a, b, c** show 3D maps of the change in absorbance (ΔA) plotted as a

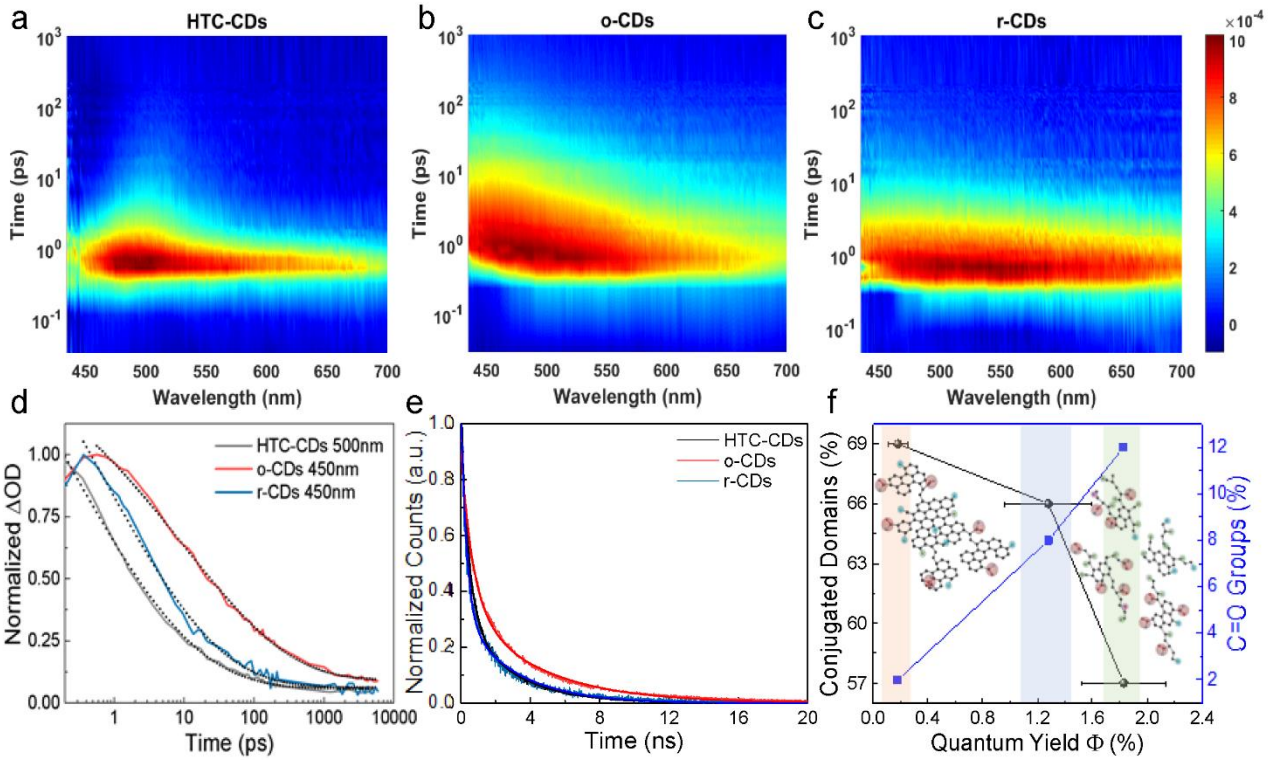

Figure 3 Femtosecond TA spectral maps of (a) o-CDs (b) r-CDs (c) HTC-CDs normalized to HTC-CDs spectra, and corresponding kinetics at (d) 450 nm for o-CDs/r-CDs, 500 nm for HTC-CDs with 360 nm pump;(e) TCSPC emission decays at 500 nm fitted with a bi-exponential function; results from fits are presented in **Table 2**; (f) Summarizes the interplay between quantum yield (Φ) and XPS percent density of the conjugated sp^2 carbon and C=O groups

To gain insights on the excited state properties of the CDs, we carried out time-resolved photoluminescence and absorption spectroscopic studies. Time-correlated single photon counting (TCSPC) was used to measure the PL lifetimes of CDs by employing a 405 nm laser excitation and probing at 440, 500, 550 and 600 nm. The resulting PL decays measured at 500 nm are included in **Figure 3e**, whilst the rest are included in **Figure S7**. The 500 nm decays were best fitted with a bi-exponential function yielding sub-nanosecond and nanosecond time constants (**Table 2**), matching previously published PL lifetimes of CDs.[12,42,45] Our data show that o-CDs have the longest-lived PL whilst HTC-CDs the shortest-lived, contradicting the trend in Φ measured by us and ranking r-CDs as the least emissive system out the three studied. Similar discrepancies between lifetimes and Φ have been observed for CDs and indicate that fluorescence lifetimes

function of time and probe wavelength for o-CDs, r-CDs and HTC-CDs, correspondingly. The maps reveal a broad excited state absorption (ESA) signal with a distinctly different spectral shape and dynamic for each of the CDs agreeing with their different Φ and structural properties. Stimulated emission was not clearly observed due to the CD's low Φ, although such signals may be over imposed on the positive ESA.[39,45,48] From **Figure 3a**, we find that the ESA of o-CDs undergoes a sub-picosecond peak shift of > 0.4 eV which is followed by peak narrowing producing a low intensity signal (< 5 %) with a maximum at ~ 450 nm. This ultrafast process can be interpreted as energy transfer through a density of states or an excited state vibrational relaxation generating localized emissive

excited states and causing the Stokes shift detected by our PL experiments. Such shifting and dynamics are not clearly dominant in the spectra of r-CDs and HTC-CDs, at least within our instrument response function, but instead their ESA dynamics indicates much faster excited state relaxation and a lower yield of generated long-lived localized excited states. Therefore, these data suggest that the reduced rigidity of the o-CDs compared to r-CDs and HTC-CDs and their increased concentration of C=O groups is clearly beneficial for enhancing their Φ.

Table 2 Results from least square fitting of the transient absorption decays at 450 and 500 nm using a stretched exponential function and the TCSPC emission decays at 500 nm using a bi-exponential function.

Sample	wavelength	τ_1 (ps)		b	
TAS					
HTC-CDs	500 nm	0.20		0.23	
o-CDs	450 nm	9.92		0.28	
r-CDs	450 nm	0.69		0.26	
TCSPC	wavelength	A1	τ1 (ns)	A2	τ1
HTC-CDs	500 nm	69%	0.46	31%	2.8
o-CDs	500 nm	62%	0.69	38%	4.28
r-CDs	500 nm	65%	0.33	35%	3.04

Unlike previous ultrafast spectroscopy studies of CDs, fitting of the ESA decay kinetics was successful both with a stretched exponential and a 3-exponential function,[12,40,49] thereby, providing little extra information about the nature of the competing relaxation processes in this system, but giving us a good indication of the average timescale of excited state decay to compare between CDs. **Table 2** presents the results from our least square fitting with the stretched exponential function $\Delta A \sim \exp-(t/\tau)^{\beta}$, where β is the stretching exponent, τ is the decay time constant and t is time. The results show that light absorption by o-CDs leads to a dominant ultrafast excited state decay with a τ = 9.9 ps and β = 0.28 indicating a rather large distribution of decay constants and ultrafast excited state relaxation. Such ultrafast excited state decay dynamics are typical for graphene and graphene oxide and previously assigned to phonon-assisted relaxation to ground state through the density of states of the sp^2 carbon network.[40,49–51] According to our results, the non-radiative relaxation is an order of magnitude faster in r-CDs than in o-CDs agreeing with the differences in Φ between these systems and indicating that the increased graphitic structure of r-CDs is the main cause of this sample's weaker PL.

To analyse the excitation wavelength dependence in the excited state properties of the CDs, as seen from the PL spectra in **Figure S6**, we recorded the transient absorption spectra of the CDs using an excitation of 310 nm. Comparing between the 310 and 360 nm spectra (**Figure S8**), we observe that the ESA is longer lived and with less pronounced trapping into localized emissive states for the shorter wavelength excitation. This behaviour supports our peak assignment of the transitions in the steady-state absorption spectra near 300 nm to predominantly π-π* transitions populating the sp^2 graphitic carbon core of the CDs, whereas excitation at longer wavelengths populates localized emissive excited states. It also shows that the interactions between these two-types of chromophores is weak and that excitation of the core states leads to ultrafast non-radiative relaxation to the ground state instead of energy transfer or internal conversion to localized emissive states. In addition, the non-radiative relaxation from the core states is slower for higher energy photon excitations as can be expected for phonon-assisted internal conversion processes.

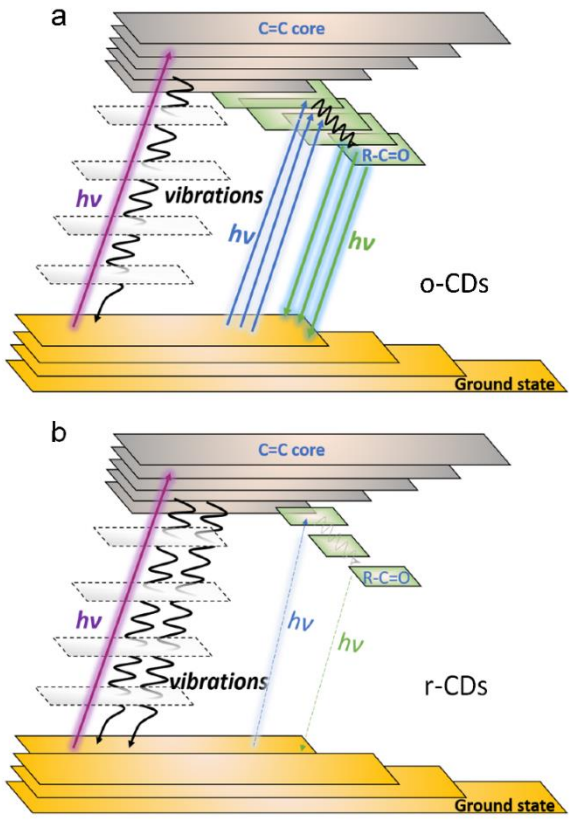

Figure 4 Excited state diagrams of (a) o-CDs and (b) r-CDs depicting the branching ratio between excited states of non-emissive sp^2 C=C graphitic carbon and emissive C=O groups.

Based on the findings from our spectroscopic study, we can now propose the relaxation process diagram of the o-CDs and r-CDs **(Figure 4)**, in which we identify that there are two main types of excited state chromophores loosely defined as sp^2 core state and C=O groups. The higher amount of graphitic structure in r-CDs causes excitation of the CDs to be predominantly into states delocalised over the sp^2 graphitic carbon which then leads to dominant non-radiative phonon-assisted internal conversion to ground states in this system, resulting in low Φ. In o-CDs, the ratio between sp^2 and C=O fluorophores has changed and the higher concentration of oxygenated groups leads to an order of magnitude higher Φ and longer lifetimes, either of which would favour their application in photocatalytic or optoelectronic applications.

Conclusions

In this paper, the structure and surface states of hydrothermally synthesized carbon dots were altered by chemical oxidization and reduction treatments. Morphological and structural studies using TEM and XPS demonstrate that compared to the as-prepared carbon dots (HTC-CDs), the oxidized carbon dots (o-CDs) possess a more amorphous and disordered structure including an increased amount of C=O and COOH functional groups, while the reduced carbon dots (r-CDs) show more graphitic and ordered structure arising from the partial restoration of sp^2 carbon structure. The UV-Vis absorbance and photoluminescence were affected by changes in their structure,

leading to an increase in the quantum yield for o-CDs and a decrease in the quantum yield of r-CDs. However, the PL emission profiles and peak broadening in o-CDs and r-CDs are similar indicating that they have similar emission centres. We identify that these centres act as individual chromophores on the nanosecond timescale and their excited states involve C=O functional groups. TAS and TCSPC techniques were used to directly probe the dynamics of formation and recombination of these centres. The results from these experiments are consistent with the existence of competing ultrafast excited state relaxation processes leading to either excited state trapping into the emissive centres or relaxation to the ground state *via* phonon-assisted internal conversion. The latter processes become faster and more dominant for r-CDs because of their increased graphitic structure, whereas it is an order of magnitude slower in o-CDs allowing for excited state trapping into the emissive excited states.

This paper sheds light on the importance of investigating how fine changes in the structure of carbon dots can induce significant changes in their optical properties and can help develop simple chemical methods to tailor these properties for specific applications in bio-labelling, optoelectronics and photocatalysis. This is very important as currently in the literature, the term “carbon dots” is used without any quantification which makes it rather difficult to unify these very different materials. We show that there are clear differences even within the same class of carbon dots, as exemplified here by the hydrothermally carbonized carbon dots and how understanding their detailed structure is crucial for controlling their optical properties. Future work would focus on tailoring the structure and PL performance of hydrothermal carbon dots (size, number and type of functional groups and graphitic character) for practical applications with focus on photocatalysis.

Conflicts of interest

The authors declare no conflicts of interest.

Acknowledgements

H. Luo thanks the Chinese government for the award of CSC scholarships, and Dr. Harold Toms for acquiring the solid- state NMR spectra. SD is grateful for financial support by Edinburgh Instruments. This work is part-funded by the European regional Development Fund through the Welsh Government. We thank the Diamond Light Source for access and support in use of the electron Physical Science Imaging Centre (Instrument E01 proposal EM17587) that contributed to the results presented here.

Notes and references

1 X. Xu, R. Ray, Y. Gu, H. J. Ploehn, L. Gearheart, K. Raker and W. A. Scrivens, *J. Am. Chem. Soc.*, 2004, **126**, 12736–12737.

2 M. Han, S. Zhu, S. Lu, Y. Song, T. Feng, S. Tao, J. Liu and B. Yang, *Nano Today*, 2018, **19**, 201–218.

3 S. N. Baker and G. A. Baker, *Angew. Chemie - Int. Ed.*, 2010, **49**, 6726–6744.

4 R. Wang, K.-Q. Lu, Z.-R. Tang and Y.-J. Xu, *J. Mater. Chem. A*, 2017, **5**, 3717–3734.

5 G. A. M. Hutton, B. C. M. Martindale and E. Reisner, *Chem. Soc. Rev.*, 2017, **46**, 6111–6123.

6 P. G. Luo, S. Sahu, S.-T. Yang, S. K. Sonkar, J. Wang, H. Wang, G. E. LeCroy, L. Cao and Y.-P. Sun, *J. Mater. Chem. B*, 2013, **1**, 2116–2127.

7 Y. Wang and A. Hu, *J. Mater. Chem. C*, 2014, **2**, 6921–6939.

8 S. Kellici, J. Acord, K. E. Moore, N. P. Power, V. Middelkoop, D. J. Morgan, T. Heil, P. Coppo, I.-A. Baragau and C. L. Raston, *React. Chem. Eng.*, 2018, **3**, 949–958.

9 Y. Dong, J. Shao, C. Chen, H. Li, R. Wang, Y. Chi, X. Lin and G. Chen, *Carbon N. Y.*, 2012, **50**, 4738–4743.

10 H. Nie, M. Li, Q. Li, S. Liang, Y. Tan, L. Sheng, W. Shi and S. X. A. Zhang, *Chem. Mater.*, 2014, **26**, 3104–3112.

11 L. Pan, S. Sun, A. Zhang, K. Jiang, L. Zhang, C. Dong, Q. Huang, A. Wu and H. Lin, *Adv. Mater.*, 2015, **27**, 7782–7787.

12 V. Strauss, J. T. Margraf, C. Dolle, B. Butz, T. J. Nacken, W. Bauer, W. Peukert, E. Spiecker, T. Clark and D. M. Guldi, *J. Am. Chem. Soc.*, 2014, **49**, 17308–17316.

13 J. T. Margraf, V. Strauss, D. M. Guldi and T. Clark, *J. Phys. Chem. B*, 2015, **119**, 7258–7265.

14 S. Zhu, Y. Song, X. Zhao, J. Shao, J. Zhang and B. Yang, *Nano Res.*, 2015, **8**, 355–381.

15 D. Pan, J. Zhang, Z. Li, C. Wu, X. Yan and M. Wu, *Chem. Commun.*, 2010, **46**, 3681.

16 Y. P. Sun, B. Zhou, Y. Lin, W. Wang, K. A. S. S. Fernando, P. Pathak, M. J. Meziani, B. A. Harruff, X. Wang, H. Wang, P. G. Luo, H. Yang, M. E. Kose, B. Chen, L. M. Veca and S. Y. Xie, *J. Am. Chem. Soc.*, 2006, **128**, 7756–7757.

17 M. Fu, F. Ehrat, Y. Wang, K. Z. Milowska, C. Reckmeier, A. L. Rogach, J. K. Stolarczyk, A. S. Urban and J. Feldmann, *Nano Lett.*, 2015, **15**, 6030–6035.

18 B. Zhu, S. Sun, Y. Wang, S. Deng, G. Qian, M. Wang and A. Hu, *J. Mater. Chem. C*, 2013, **1**, 580–586.

19 A. Marinovic, L. S. Kiat, S. Dunn, M. M. Titirici and J. Briscoe, *ChemSusChem*, 2017, **10**, 1004–1013.

20 N. Papaioannou, A. Marinovic, N. Yoshizawa, A. E. Goode, M. Fay, A. Khlobystov, M. Titirici and A. Sapelkin, *Sci. Rep.*, 2018, **8**, 6559.

21 A. C. Ferrari and J. Robertson, *Phys. Rev. B*, 2000, **61**, 14 295.

22 B. C. M. Martindale, G. A. M. Hutton, C. A. Caputo, S. Prantl, R. Godin, J. R. Durrant and E. Reisner, *Angew. Chemie - Int. Ed.*, 2017, **56**, 6459–6463.

23 C. V. V Pham, M. Krueger, M. Eck, S. Weber and E. Erdem, *Appl. Phys. Lett.*, 2014, **104**, 3–8.

24 G. Sandeep Kumar, R. Roy, D. Sen, U. K. Ghorai, R. Thapa, N. Mazumder, S. Saha and K. K. Chattopadhyay, *Nanoscale*, 2014, **6**, 3384–3391.

25 M. C. Ortega-Liebana, N. X. Chung, R. Limpens, L. Gomez, J. L. Hueso, J. Santamaria and T. Gregorkiewicz, *Carbon N. Y.*, 2017, **117**, 437–446.

26 Z. Zhang, J. Zhang, N. Chen and L. Qu, *Energy Environ. Sci.*, 2012, **5**, 8869–8890.

27 Y. Wang, S. Kalytchuk, Y. Zhang, H. Shi, S. V. Kershaw and A. L. Rogach, *J. Phys. Chem. Lett.*, 2014, **5**, 1412–1420.

28 M. Sudolská, M. Dubecký, S. Sarkar, C. J. Reckmeier, R.

Zbořil, A. L. Rogach and M. Otyepka, *J. Phys. Chem. C*, 2015, **119**, 13369–13373.
29 G. Eda, Y. Y. Lin, C. Mattevi, H. Yamaguchi, H. A. Chen, I. S. Chen, C. W. Chen and M. Chhowalla, *Adv. Mater.*, 2010, **22**, 505–509.
30 Y. Zhou, Q. Bao, L. A. L. Tang, Y. Zhong and K. P. Loh, *Chem. Mater.*, 2009, **21**, 2950–2956.
31 G. Eda and M. Chhowalla, *Adv. Mater.*, 2010, **22**, 2392–2415.
32 R. Y. N. Gengler, D. S. Badali, D. Zhang, K. Dimos, K. Spyrou, D. Gournis and R. J. D. Miller, *Nat. Commun.*, 2013, **4**, 1–5.
33 F. Ehrat, S. Bhattacharyya, J. Schneider, A. Löf, R. Wyrwich, A. L. Rogach, J. K. Stolarczyk, A. S. Urban and J. Feldmann, *Nano Lett.*, 2017, **17**, 7710–7716.
34 L. Đorđević, F. Arcudi, A. D'Urso, M. Cacioppo, N. Micali, T. Bürgi, R. Purrello and M. Prato, *Nat. Commun.*, 2018, **9**, 3442.
35 S. Zhu, Q. Meng, L. Wang, J. Zhang, Y. Song, H. Jin, K. Zhang, H. Sun, H. Wang and B. Yang, *Angew. Chemie - Int. Ed.*, 2013, **52**, 3953–3957.
36 Y. Yang, J. Cui, M. Zheng, C. Hu, S. Tan, Y. Xiao, Q. Yang and Y. Liu, *Chem. Commun.*, 2012, **48**, 380–382.
37 Q. Liang, W. Ma, Y. Shi, Z. Li and X. Yang, *Carbon N. Y.*, 2013, **60**, 421–428.
38 S. Sahu, B. Behera, T. K. Maiti and S. Mohapatra, *Chem. Commun.*, 2012, **48**, 8835.
39 L. Wang, S. J. Zhu, H. Y. Wang, S. N. Qu, Y. L. Zhang, J. H. Zhang, Q. D. Chen, H. L. Xu, W. Han, B. Yang and H. B. Sun, *ACS Nano*, 2014, **8**, 2541–2547.
40 L. Sui, W. Jin, S. Li, D. Liu, Y. Jiang, A. Chen, H. Liu, Y. Shi, D. Ding and M. Jin, *Phys. Chem. Chem. Phys.*, 2016, **18**, 3838–3845.
41 C. Galande, A. D. Mohite, A. V Naumov, W. Gao, L. Ci, A. Ajayan, H. Gao, A. Srivastava, R. B. Weisman and P. M. Ajayan, *Sci. Rep.*, 2011, **1**, 85.
42 M. O. Dekaliuk, O. Viagin, Y. V. Malyukin and A. P. Demchenko, *Phys. Chem. Chem. Phys.*, 2014, **16**, 16075–16084.
43 B. Ghosh, M. Takeguchi, J. Nakamura, Y. Nemoto, T. Hamaoka, S. Chandra and N. Shirahata, *Sci. Rep.*, 2016, **6**, 36951.
44 R. Kirmse, *Magn. Reson. Chem.*, 1995, **33**, 698.
45 V. Strauss, A. Kahnt, E. M. Zolnhofer, K. Meyer, H. Maid, C. Placht, W. Bauer, T. J. Nacken, W. Peukert, S. H. Etschel, M. Halik and D. M. Guldi, *Adv. Funct. Mater.*, 2016, **26**, 7975–7985.
46 A. Jaiswal, S. S. Ghosh and A. Chattopadhyay, *Chem. Commun.*, 2012, **48**, 407–409.
47 X. Wang, K. Qu, B. Xu, J. Ren and X. Qu, *Nano Res.*, 2011, **4**, 908–920.
48 L. Wang, S. J. Zhu, H. Y. Wang, Y. F. Wang, Y. W. Hao, J. H. Zhang, Q. D. Chen, Y. L. Zhang, W. Han, B. Yang and H. B. Sun, *Adv. Opt. Mater.*, 2013, **1**, 264–271.
49 X. Wen, P. Yu, Y. R. Toh, X. Hao and J. Tang, *Adv. Opt. Mater.*, 2013, **1**, 173–178.
50 P. George, J. Strait, J. Dawlaty, S. Shivaraman, M. Chandrashekhar, F. Rana and M. G. Spencer, *Nano Lett*, 2008, **8**, 17–20.
51 J. M. Dawlaty, S. Shivaraman, M. Chandrashekhar, F. Rana and M. G. Spencer, *Appl. Phys. Lett.*, 2008, **92**, 042116.